Extracting Lagrangian coherent structures in cardiovascular flows using Lagrangian descriptors

Cite as: Phys. Fluids **33**, 111707 (2021); https://doi.org/10.1063/5.0064023 Submitted: 19 July 2021 • Accepted: 07 October 2021 • Published Online: 16 November 2021

🗓 Ahmed Darwish, 🗓 Shahrzad Norouzi, 🗓 Giuseppe Di Labbio, et al.







ARTICLES YOU MAY BE INTERESTED IN

Flow examination in abdominal aortic aneurysms: Reduced-order models driven by in vitro data and spectral proper orthogonal decomposition

Physics of Fluids 33, 111708 (2021); https://doi.org/10.1063/5.0069560

Interactions between Görtler vortices and the second mode in hypersonic boundary layer Physics of Fluids 33, 111701 (2021); https://doi.org/10.1063/5.0073053

A predictive model of the drag coefficient of a circular cylinder Physics of Fluids **33**, 111702 (2021); https://doi.org/10.1063/5.0071079

Physics of Fluids
Special Topic: Cavitation





Extracting Lagrangian coherent structures in cardiovascular flows using Lagrangian descriptors

Cite as: Phys. Fluids 33, 111707 (2021); doi: 10.1063/5.0064023 Submitted: 19 July 2021 · Accepted: 7 October 2021 · Published Online: 16 November 2021















AFFILIATIONS

- Laboratory of Cardiovascular Fluid Dynamics, Concordia University, Montréal, Quebec H3G 1M8, Canada
- ²Mechanical Engineering Department, Assiut University, Assiut 71515, Egypt
- ³Laboratoire de dynamique des fluides, Polytechnique Montréal, Montréal, Quebec H3C 3A7, Canada
- ⁴Département de génie mécanique, École de technologie supérieure, Montréal, Quebec H3C 1K3, Canada

ABSTRACT

In cardiovascular flows, Lagrangian coherent structures have been used to explore the skeleton of blood transport. Revealing these transport barriers is instrumental to quantify the mixing and stagnation of blood as well as to highlight locations of elevated strain rate on blood elements. Nevertheless, the clinical use of Lagrangian coherent structures in cardiovascular flows is rarely reported due largely to its nonintuitive nature and computational expense. Here, we explore a recently developed approach called "Lagrangian descriptors," which quantifies the finite time Euclidean arc length of Lagrangian trajectories released from a grid of initial positions. Moreover, the finite time arc lengths of a set of trajectories capture signatures of Lagrangian coherent structures computed from the same initial condition. Remarkably, the Lagrangian descriptors approach has the most rapid computational performance among all its Lagrangian counterparts. In this work, we explore the application of Lagrangian descriptors for the first time in cardiovascular flows. For this purpose, we consider two in vitro flow models studied previously by our group: flow in an abdominal aortic aneurysm and that in a healthy left ventricle. In particular, we will demonstrate the ability of the Lagrangian descriptors approach to reveal Lagrangian coherent structures computed via the classical geometrical approach, though at a significantly reduced computational cost.

Published under an exclusive license by AIP Publishing. https://doi.org/10.1063/5.0064023

Blood mixing, separation, and stasis in cardiovascular flows can be better understood by revealing the underlying mechanism or skeleton of blood transport. This transport skeleton has been obtained in a variety of cardiovascular flows by extracting coherent structures. 1-3 One way to perform such a task is to extract the Lagrangian coherent structures (LCSs), which describe highly repelling, attracting, and shearing material lines/surfaces within various time-dependent flows.^{4–9} In addition to providing a map of material (blood) transport within a cardiovascular flow, LCSs can be used to capture the boundaries of vortical structures and show how they are transported.² Furthermore, extracting LCS in blood flows has different applications such as optimizing and controlling the targeted drug delivery, 15 to examine the effectiveness of diverter stent on patients with intracranial aneurysm,¹⁷ to predict the growth of abdominal aortic aneurysm (AAA). Moreover, Shadden and Taylor suggest that a higher degree of stirring and mixing is associated with a more complex distribution

of LCSs within a given flow region. They also found a correlation between the boundary of stagnant flow and a repelling LCS within an idealized model of AAA. Another important application of LCSs relies on their nature as the most attracting/repelling material surfaces. Specifically, platelets located on LCSs will experience higher strain rates, opening the door for their potential activation.^{3,1}

In the literature, several approaches can be used to deduce LCSs within flows, the more common being geometric, probabilistic, braidbased, and trajectory-graph based.^{20–22} Among these approaches, the geometric approach has been extensively used to define LCSs within cardiovascular flows. Central to this approach is finding the largest eigenvalue of the right Cauchy-Green tensor (CGT), which indicates the maximum amount of stretching at a given initial point in a fluid domain. Often, the right CGT is computed for a dense grid of particles with their trajectories being traced between two time instants. Then, after rescaling the largest eigenvalue field, the finite-time Lyapunov

^{a)}Author to whom correspondence should be addressed: lcfd@encs.concordia.ca and ahmeddiaa@aun.edu.eg

exponent (FTLE) field can be used to visualize the LCSs within the flow. The reader can anticipate that such an approach is computationally expensive as it requires a dense grid of Lagrangian trajectories along with highly resolved spatial derivatives of the flow map. Therefore, although the geometric approach (i.e., using the FTLE fields) can identify the LCS, it has been shown to give a blurry view of the stable and unstable manifolds of hyperbolic trajectories in oceanographic flows.²³

Lagrangian descriptors (LD) is a trajectory-based diagnostic technique that has emerged as a means of overcoming the computationally demanding nature of geometric approaches to more easily visualize LCSs.^{23–27} According to Mendoza and Mancho,²⁵ a function is proposed as a global LD, where this function evaluates the finite time Euclidean arc length of a Lagrangian trajectory originating from a given initial position in the flow. As the attracting and repelling LCSs partition the fluid into regions with different dynamics, one can expect that the lengths of the trajectories will witness abrupt changes in their vicinity.²⁵ Moreover, Mancho *et al.*²⁸ extended LD to include the finite time integration of scalar properties (either geometrical or physical) along the trajectories. Thus, in fluid flows, the sharp gradient in the Lagrangian descriptors can deduce the attracting and repelling LCSs.^{21,29,30}

To extract LCSs within cardiovascular flows, the most common approach has been the geometrical one. A faster LCS detection algorithm would open the door to its application to cardiovascular flows acquired in a clinical setting via four-dimensional (4D) MRI or echo-Particle image velocimetry (PIV). It is therefore important to demonstrate that the LD approach is an excellent candidate for this purpose. In order to do so, the LD approach is here applied to two cardiovascular flow fields acquired from experimental *in vitro* models of flow in a healthy left ventricle (LV) and that in an AAA. Since the two selected flows are rich with complex LCSs, we will demonstrate the ability of the LD approach to extract the same LCSs highlighted by the FTLE fields. Moreover, we will show the significant computational savings that the LD approach offers.

Starting with a time-dependent velocity field $\mathbf{u}(\mathbf{x},t)$, we place a set of uniformly spaced passive particles over a grid at a given time t_0 .

Then, the Lagrangian trajectories are traced by advecting the particles in time using a fourth-order Runge–Kutta scheme along with a bicubic spatial interpolation of the velocity fields. By doing so, we ensure an efficient and accurate computation of the trajectories as reported in Mendoza *et al.*²⁷

For a given Lagrangian trajectory that passes through a position \mathbf{x}_0 at time t_0 , the Euclidean arc length of this trajectory, for a given time interval τ , defines the value of the Lagrangian descriptors through a function $\mathbf{M}(\mathbf{x}_0, t_0, \tau)$ as in Madrid and Mancho.²⁴ Here, we use the discrete form of M (denoted hereafter as DM) as defined by Lopesino et al., where the Lagrangian trajectory is defined over 2N + 1 time steps, with $N \in \mathbb{N}$. In the literature, Eq. (1) represents the Lagrangian descriptors for a trajectory i by summing the expressions given by Eqs. (2) and (3). The forward DM (DM^F) is computed for the trajectory originating from \mathbf{x}_0 between t_0 and $t_0 + \tau_F$ while the backward DM $(\mathbf{D}\mathbf{M}^B)$ is evaluated for the trajectory ending at \mathbf{x}_0 from $t_0 - \tau_B$ to t_0 , see panel II in Fig. 1. In this case, if Δt represents the time step between the investigated velocity fields, the time interval can be defined as $\tau = N\Delta t$. Notably, the following expressions differentiate between the number of time steps for both forward and backward computations of the DM:

$$DM_{i} = DM_{i}^{F} + DM_{i}^{B} = \sum_{n=-N_{B}}^{N_{F}} \sqrt{(x_{i}^{n+1} - x_{i}^{n})^{2} + (y_{i}^{n+1} - y_{i}^{n})^{2}}, (1)$$

$$DM_i^F = \sum_{n=0}^{N_F} \sqrt{(x_i^{n+1} - x_i^n)^2 + (y_i^{n+1} - y_i^n)^2},$$
 (2)

$$DM_i^B = \sum_{n=-N_B}^{0} \sqrt{(x_i^{n+1} - x_i^n)^2 + (y_i^{n+1} - y_i^n)^2}.$$
 (3)

The repelling and attracting LCSs can be captured by finding locations with sharp gradients in the **DM** contours (as in panel III in Fig. 1). This can be justified by considering trajectories that start nearby each other and continue their temporal evolution close to each other; thus, their Euclidean arc lengths (i.e., DM value) do not vary

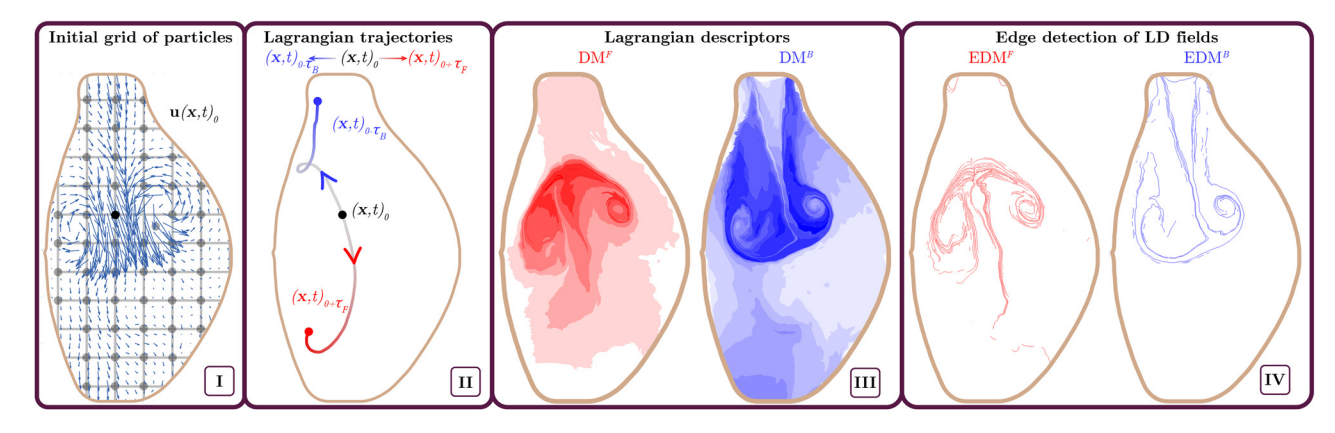


FIG. 1. Illustration of the LD approach to extract LCS in cardiovascular flows. Panel (I) shows the initial grid of particles that will be used to trace the Lagrangian trajectories inside the AAA model. The particles are released at initial time t_0 , which corresponds to initial velocity field $\mathbf{u}(\mathbf{x},t)_0$. Panel (II) shows a single Lagrangian trajectory obtained by tracing the particle forward and backward in time. The trajectory has a colored gradient indicating the value of its Euclidean arc length. Fade color indicates smaller length while dark blue and dark red indicates higher arc length. In panel (III), the two functions \mathbf{DM}^F and \mathbf{DM}^B are evaluated at each initial location. Here, dark red and dark blue indicate higher trajectory length in forward and backward directions, respectively. In panel (IV), we show the application of the Sobel filter to extract the edge of the DM contours, where the red and blue edges are aligned with the repelling and attracting LCS, respectively.

significantly if they belong to a flow region with the same dynamics. However, at the vicinity of LCS (i.e., separating flow regions with different dynamics), one may expect that the trajectory coinciding with these structures will witness abrupt change in its DM value relative to other nearby trajectories, as defined in Ref. 24. Thus, the locations of sharp color gradient are called singular features of the Lagrangian descriptors and are aligned with the repelling LCSs (in \mathbf{DM}^F) and the attracting LCSs (in \mathbf{DM}^B). 23,29,30 To accurately locate the singular features of the \mathbf{DM} map, García-Garrido suggested using a Sobel filter, which can identify the edges at locations where the gradient of \mathbf{DM} is maximum. The detected edges are stored in a new two-dimensional field called \mathbf{EDM} "indicating the edge of the DM field" as shown in panel IV of Fig. 1.

Conceptually, the FTLE field represents the maximum exponential separation rate of a closely spaced pair of particles being advected in a flow over a given time interval τ . For a fluid domain within a time-dependent velocity field $\mathbf{u}(\mathbf{x},t)$, trajectories $\mathbf{x}(t;t_0,\mathbf{x}_0)$ are followed for a very large number of particles with initial positions \mathbf{x}_0 . The flow map $\mathcal{F}_{t_0}^{t_0+\tau}$: $\mathbf{x}(t_0) \mapsto \mathbf{x}(t_0) + \int_{t=t_0}^{t_0+\tau} \mathbf{u}(\mathbf{x}(\mathbf{t}_0),t_0+\tau)dt$ moves the particles between their initial and future positions after a time interval τ . The right CGT Δ is then given by Eq. (4), where $\mathbf{D}\mathcal{F}_{t_0}^{t_0+\tau}$ denotes the Jacobian of the flow map. As the CGT measures the amount of particle separation or material stretching at each initial position, the maximal stretching is aligned with the eigenvector corresponding to the maximum eigenvalue λ_{max} of the CGT. The FTLE, as given by

Eq. (5), then corresponds to a rescaling of the maximum eigenvalues and can be used to visualize LCSs in the flow.

$$\Delta_{t_0}^{t_0+\tau}(\mathbf{x}) = \left[\mathbf{D} \mathcal{F}_{t_0}^{t_0+\tau} \right]^* \left[\mathbf{D} \mathcal{F}_{t_0}^{t_0+\tau} \right], \tag{4}$$

$$\sigma_{t_0}^{\tau}(\mathbf{x},t) = \frac{1}{2|\tau|} \ln \lambda_{\max}(\Delta_{t_0}^{t_0+\tau}(\mathbf{x})). \tag{5}$$

The first application of the LD approach, in this study, includes a model of an AAA. A recently developed *in vitro* simulator ³³ generates a physiological flow inside the AAA model as shown in the left panel of Fig. 2. The velocity fields are measured using time-resolved planar particle image velocimetry with a spatial resolution of 0.6 mm and a temporal resolution of 1.9 $\times 10^{-3}$ s. Since both the DM and FTLE fields depend on advecting a set of an initial grid of particles at time t_0 , all reported computations use the same fine grid of particles and time intervals (τ_F and τ_B). The initial grid of particles is refined eight times from the original grid to ensure a high resolution of the reported structures. The initial release time of the particles is $t_0=0.4$, while time intervals of $\tau_B=0.42$ and $\tau_F=0.6$ are used for the evaluation of DM as given by Eqs. (2) and (3), respectively.

The second investigated flow is that inside a model of the LV where, similar to the AAA case, an *in vitro* simulator is used to generate healthy flow conditions as shown in the right panel of Fig. 2.³⁴ The flow was originally acquired using particle image velocimetry and reduced-order models have been made available so with a temporal

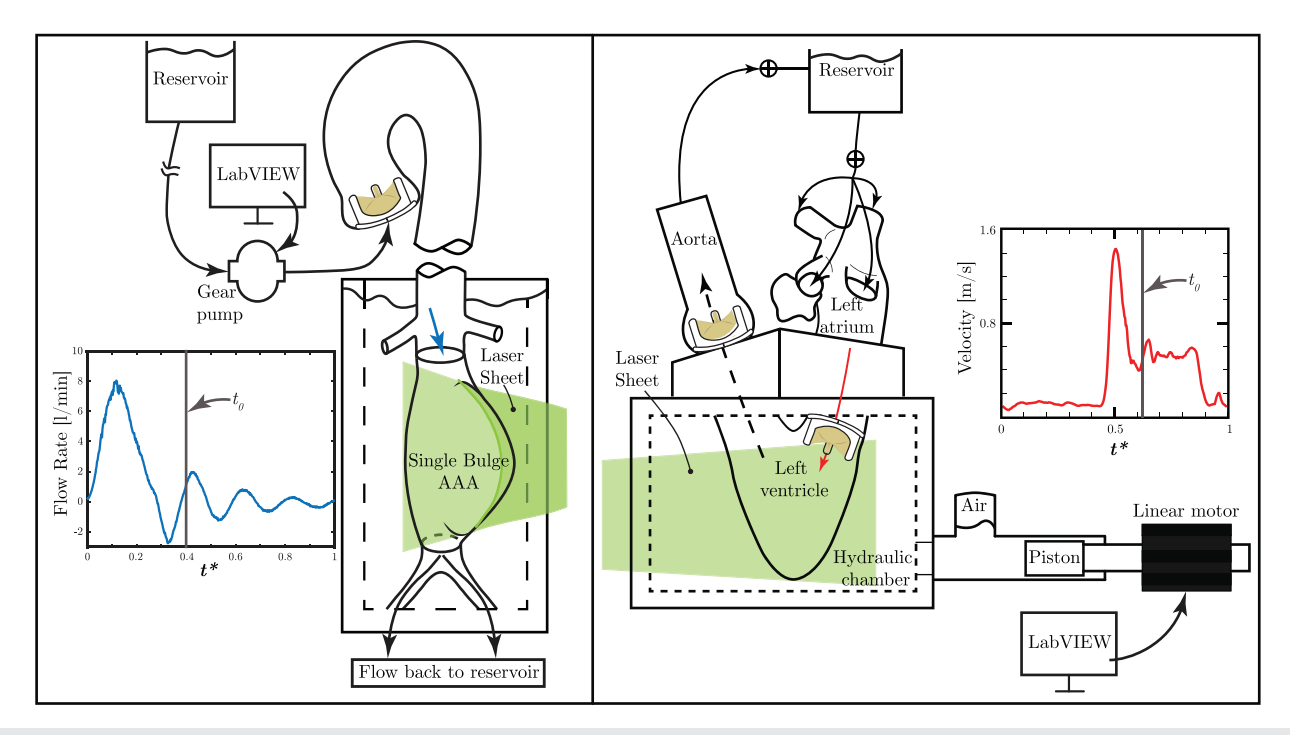


FIG. 2. Left panel shows the *in vitro* setup being used to generate and quantify the flow in the AAA model. The plane of PIV measurements is highlighted in green. A gear pump generates the flow inside the AAA model, where the pump is driven by a LabVIEW controlled motor. The flow waveform at the inlet of the AAA model is shown in blue with the initial release time t_0 of the particles being indicated by the vertical gray line. In the right panel, we show the *in vitro* setup that has been used to generate the healthy flow inside the LV model. The intra-ventricular flow is generated by controlling the pressure inside the hydraulic chamber. This task is done by moving the piston attached to a LabVIEW controlled linear motor. The inlet velocity profile at the mitral side is shown by the red curve while the initial release time of particles for our investigation is indicated by the vertical gray line.

resolution of 2.5×10^{-3} s and a spatial resolution of 1.04 mm. The initial grid of advected particles is eight times finer than the original grid and advection is started at time $t_0=0.62$. At this time, the rapid filling jet becomes clearly present inside the LV. Moreover, the forward and backward time intervals are different with $\tau_B=0.11$ and $\tau_F=0.7$. Notably, using $\tau_B>t_0$ in the AAA and $\tau_F>1-t_0$ for the LV requires two cycles for the evaluation of particle trajectories. Thus, the data set holding the velocity fields for a single cycle has been appended to itself for both cases. Further details on the selection of τ can be found in the supplementary material.

Figure 3 shows the forward and backward DM, EDM, and FTLE fields for the AAA and the LV cases at initial time t_0 . By inspecting the DM maps and the FTLE fields, qualitative similarities can be observed. For instance, in the AAA, the boundaries of the propagating vortical structures are revealed by the FTLE ridges; see the last row in Fig. 3. The organization of such structures matches regions with high DM

values (dark red and dark blue) surrounded by fluid regions with sharp color gradients (toward the white). Notably, the EDM maps (obtained via the Sobel filter) closely resemble the FTLE fields. For instance, the boundaries of the vortex pair identified by the FTLE (computed forward in time) are clearly captured by the EDM. Similarly, the backward EDM field detects various structures that are identified by the backward FTLE field. For instance, the V-shaped structure descending from the AAA inlet in addition to the vortical structures are well detected.

As the LV flow has more complex structures, the DM maps (both forward and backward) show larger regions defined by sharp gradients particularly in the \mathbf{DM}^F map. On the other hand, the \mathbf{DM}^B map shows the boundary of the rolling vortex with high descriptor values surrounded by a spiral of low values. As for the AAA, the EDM and FTLE fields for the LV case show similarities. For instance, the edges of the backward EDM field are aligned with the FTLE fields as

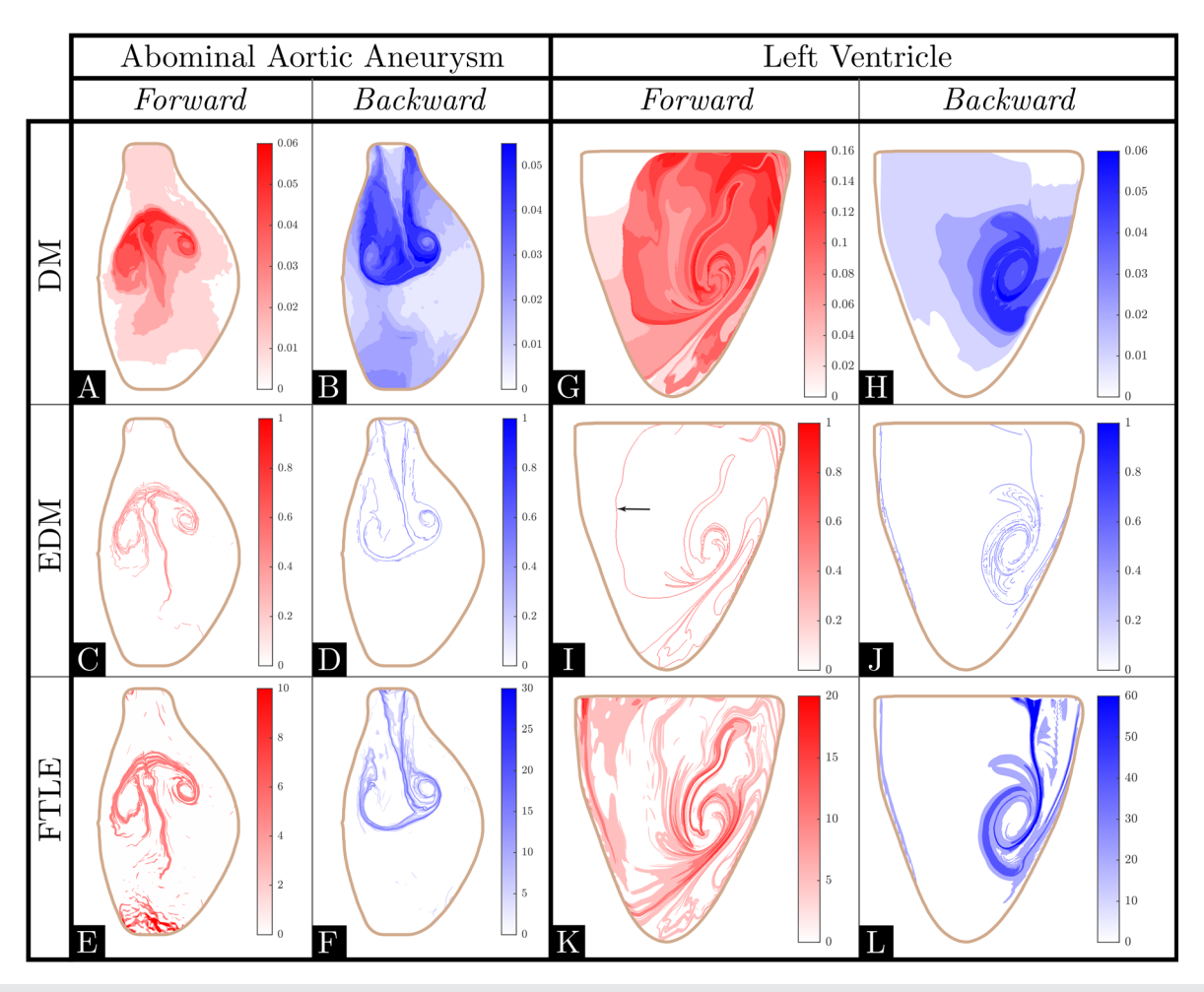


FIG. 3. A comparison between the contours of DM, EDM, and FTLE for the two investigated flows. DM represents the contours of the Discrete M function that evaluates the Lagrangian descriptors. EDM shows the detected edges of DM contours using a Sobel filter. FTLE represents the repelling and attracting LCS for forward and backward finite time interval. The two columns under the abdominal aortic aneurysm panel are evaluated at $t_0 = 0.4$, $\tau_F = 0.42$ and $\tau_B = 0.6$. For the LV flow, $t_0 = 0.62$, $\tau_F = 0.7$, and $\tau_B = 0.11$. The sharp gradients in the DM contours (A, B, G, H) show clear imprint of the ridges being highlighted in the FTLE fields in (E, F, K, L). The location of sharp gradients in DM are revealed by the EDM contours as in (C, D, I, J), which clearly resemble the opposite FTLE fields. Multimedia views: https://doi.org/10.1063/5.0064023.1; https://doi.org/10.1063/5.0064023.2; https://doi.org/10.1063/5.0064023.3; https://doi.org/10.1063/5.0064023.3; https://doi.org/10.1063/5.0064023.3

shown in Fig. 3. The similarity between the forward EDM and FTLE fields is also sustained; however, the EDM reveals a relatively long vertical edge (indicated by the black arrow in Fig. 3), which has no trace in the FTLE field.

To notice the temporal evolution of forward and backward EDM maps, the reader can see videos 1 and 2 for the AAA flow, while videos 3 and 4 show the same maps for the LV flow (Fig. 3, Multimedia views).

As all computational parameters are similar between the DM and the FTLE field, we quantify the computational time per time interval for each case. The computations are performed on a computer with an Intel Core i7–6700 processor running at 3.4 GHz using 32.0 GB of RAM running on Windows 10 64-bit operating system. We observe that the LD approach significantly decreases the computational time by at least five times as reported in Table I.

In this study, we apply the Lagrangian descriptors approach to cardiovascular flows. For this purpose, we used two *in vitro* cardiovascular flows rich in complex flow structures—those in an AAA and in a healthy LV. As the Lagrangian descriptors rely on the integration of a geometrical or physical property along a given set of Lagrangian trajectories, ²⁸ here, we select the arc length of the trajectories to indicate the Lagrangian descriptors' value for a given finite time interval.

By comparing the application of the LD approach to cardiovascular and oceanographic flows, a major difference is noted in the selection for the value of the time interval τ . For instance, Mendoza and Mancho²⁶ used a single finite time interval for both forward and backward computations of **DM** in their analysis of the Kuroshio currents. For cardiovascular flow, in order to capture the attracting and repelling LCS, we had to split the DM expression into **DM**^F and **DM**^B, each being computed with a corresponding finite time interval τ_F and τ_B .

The need to use different time intervals can be related to the dynamics of the flow. For instance, Mancho et al.28 reported that shorter values of τ successfully capture structures with large repelling/ attracting nature. In this study, a similar conclusion can be drawn by inspecting the LV case. As the initial release time of the Lagrangian trajectories is shortly after the rapid filling, the mitral flow rapidly accelerates into the LV. To compute DM^B, trajectories are traced backward in time where for longer τ_B , one can expect that trajectories closer to the mitral valve will rapidly escape the flow domain. At such conditions, the DM map is reported to perturb the identified structures.³⁶ The reader can see a comparison between the backward FTLE and DM fields using incrementally increasing values of τ_B in the supplementary material. Recently, García-Garrido³⁶ suggested calculating the DM function along the trajectory until reaching the desired time interval τ or the trajectory escapes the domain. He called this approach Variable Iteration Number of Discrete Lagrangian Descriptors or

TABLE I. The elapsed computational time (in seconds) to evaluate the FTLE and the LD fields for one time step for the AAA and the LV flows.

	Computational time per time step (s) FTLE	LD
AAA	0.286	0.042
LV	0.290	0.054

VIN-DLD. Applying the VIN-DLD approach to obtain the backward DM field, in the LV flow, has not revealed additional structures.

As the sharp gradients in DM contours indicate the locations of attracting and repelling LCS, finding the gradient of DM (i.e., $||\nabla DM||)$ can accurately locate the LCS. To do so, we applied the Sobel filter to detect locations with sharp gradient of the DM field, which follows the suggestions in Ref. 31. Notably, the identified edges match to a greater extent the distribution of the FTLE ridges.

Since the major advantage of using the LD approach is its computational cost, we find it to be at least five times faster than the geometric approach (using the FTLE).

In conclusion, using two examples, we have illustrated the applicability of the Lagrangian descriptor approach to deduce LCSs in cardiovascular flows. This approach can be significantly faster than the other common LCS extraction approach (using the FTLE). By introducing such an approach to cardiovascular flows, clinical extraction of LCSs can be done rapidly with reasonable computational resources. Then, such an application can be implemented directly on cardiovascular flows being acquired clinically via 4D MRI or echo-PIV. Moreover, in real blood flows, the existing blood components can alter the distribution of the deduced structures; therefore, using clinically acquired velocity fields will ensure the accuracy of the extracted structures. Finally, performing further *in vivo* studies is required to promote using Lagrangian descriptors to extract LCS in clinical practice.

SUPPLEMENTARY MATERIAL

See the supplementary material for further discussion on the effect of the value of τ on the resulting DM maps.

ACKNOWLEDGMENTS

This work is supported by a grant from the Natural Sciences and Engineering Research Council of Canada (NSERC), No. 343164-07.

AUTHOR DECLARATIONS

Conflict of Interest

The authors have no conflicts to disclose.

DATA AVAILABILITY

The flow inside the healthy left ventricle is constructed using the reduced order models provided at https://github.com/dilabbiog/ROMs-LV_flow_with_AR, Ref. 37. The post-processing of the data is carried out using the codes in GitHub at https://github.com/dilab-biog/matfluids, Ref. 39.

REFERENCES

¹S. C. Shadden and C. A. Taylor, "Characterization of coherent structures in the cardiovascular system," Ann. Biomed. Eng. **36**, 1152–1162 (2008).

²G. D. Labbio, J. Vétel, and L. Kadem, "Material transport in the left ventricle with aortic valve regurgitation," Phys. Rev. Fluids 3, 113101 (2018).

³A. Darwish, G. D. Labbio, W. Saleh, and L. Kadem, "In vitro characterization of Lagrangian fluid transport downstream of a dysfunctional bileaflet mechanical aortic valve," AIP Adv. 10, 095319 (2020).

⁴G. Haller, "Lagrangian coherent structures," Annu. Rev. Fluid Mech. 47, 137–162 (2015).

⁵W. H. Weheliye, N. Cagney, G. Rodriguez, M. Micheletti, and A. Ducci, "Mode decomposition and Lagrangian structures of the flow dynamics in orbitally shaken bioreactors," Phys. Fluids 30, 033603 (2018).

- ⁶S.-L. Cao, X. Sun, J.-Z. Zhang, and Y.-X. Zhang, "Forced convection heat transfer around a circular cylinder in laminar flow: An insight from Lagrangian coherent structures," Phys. Fluids 33, 067104 (2021).
- ⁷X. Si and L. Fang, "Preferential alignment and heterogeneous distribution of active non-spherical swimmers near Lagrangian coherent structures," Phys. Fluids 33, 073303 (2021).
- ⁸X. Ma, Z. Tang, and N. Jiang, "Eulerian and Lagrangian analysis of coherent structures in separated shear flow by time-resolved particle image velocimetry," Phys. Fluids **32**, 065101 (2020).
- ⁹S. Qin, H. Liu, and Y. Xiang, "On the formation modes in vortex interaction for multiple co-axial co-rotating vortex rings," Phys. Fluids 30, 011901 (2018).
- ¹⁰S. C. Shadden, M. Astorino, and J.-F. Gerbeau, "Computational analysis of an aortic valve jet with Lagrangian coherent structures," Chaos: Interdiscip. J. Nonlinear Sci. 20, 017512 (2010).
- ¹¹J. Töger, M. Kanski, M. Carlsson, S. J. Kovács, G. Söderlind, H. Arheden, and E. Heiberg, "Vortex ring formation in the left ventricle of the heart: Analysis by 4D flow MRI and Lagrangian coherent structures," Ann. Biomed. Eng. 40, 2652–2662 (2012).
- ¹²M. G. Badas, F. Domenichini, and G. Querzoli, "Quantification of the blood mixing in the left ventricle using finite time Lyapunov exponents," Meccanica 52, 529–544 (2017).
- ¹³P. M. Arvidsson, S. J. Kovács, J. Töger, R. Borgquist, E. Heiberg, M. Carlsson, and H. Arheden, "Vortex ring behavior provides the epigenetic blueprint for the human heart," Sci. Rep. 6, 22021 (2016).
- ¹⁴O. Mutlu, H. E. Salman, H. C. Yalcin, and A. B. Olcay, "Fluid flow characteristics of healthy and calcified aortic valves using three-dimensional Lagrangian coherent structures analysis," Fluids 6, 203 (2021).
- ¹⁵S. S. Meschi, A. Farghadan, and A. Arzani, "Flow topology and targeted drug delivery in cardiovascular disease," J. Biomech. 119, 110307 (2021).
- ¹⁶J. Brum, M. Bernal, N. Barrere, C. Negreira, and C. Cabeza, "Vortex dynamics and transport phenomena in stenotic aortic models using echo-PIV," Phys. Med. Biol. 66, 055026 (2021).
- ¹⁷O. Mutlu, A. B. Olcay, C. Bilgin, and B. Hakyemez, "Understanding the effect of effective metal surface area of flow diverter stent's on the patient-specific intracranial aneurysm numerical model using Lagrangian coherent structures," J. Clin. Neurosci. 80, 298–309 (2020).
- ¹⁸F. Joly, G. Soulez, D. Garcia, S. Lessard, and C. Kauffmann, "Flow stagnation volume and abdominal aortic aneurysm growth: Insights from patient-specific computational flow dynamics of Lagrangian-coherent structures," Comput. Biol. Med. 92, 98–109 (2018).
- ¹⁹S. C. Shadden and S. Hendabadi, "Potential fluid mechanic pathways of platelet activation," <u>Biomech. Model. Mechanobiol.</u> 12, 467–474 (2013).
- ²⁰M. R. Allshouse and T. Peacock, "Lagrangian based methods for coherent structure detection," Chaos: An Interdiscip. J. Nonlinear Sci. 25, 097617 (2015).
- ²¹A. Hadjighasem, M. Farazmand, D. Blazevski, G. Froyland, and G. Haller, "A critical comparison of Lagrangian methods for coherent structure detection," Chaos: Interdiscip. J. Nonlinear Sci. 27, 053104 (2017).

- ²²S. Balasuriya, N. T. Ouellette, and I. I. Rypina, "Generalized Lagrangian coherent structures," Phys. D: Nonlinear Phenom. 372, 31–51 (2018).
- ²³A. de la Cámara, A. M. Mancho, K. Ide, E. Serrano, and C. R. Mechoso, "Routes of transport across the Antarctic polar vortex in the southern spring," J. Atmos. Sci. 69, 741–752 (2012).
- ²⁴J. A. J. Madrid and A. M. Mancho, "Distinguished trajectories in time dependent vector fields," Chaos: An Interdiscip. J. Nonlinear Sci. 19, 013111 (2009).
- ²⁵C. Mendoza and A. M. Mancho, "Hidden geometry of ocean flows," Phys. Rev. Lett. 105, 038501 (2010).
- ²⁶C. Mendoza and A. M. Mancho, "The Lagrangian description of aperiodic flows: A case study of the Kuroshio current," Nonlinear Processes Geophys. 19, 449–472 (2012).
- ²⁷C. Mendoza, A. M. Mancho, and S. Wiggins, "Lagrangian descriptors and the assessment of the predictive capacity of oceanic data sets," Nonlinear Processes Geophys. 21, 677–689 (2014).
- ²⁸A. M. Mancho, S. Wiggins, J. Curbelo, and C. Mendoza, "Lagrangian descriptors: A method for revealing phase space structures of general time dependent dynamical systems," Commun. Nonlinear Sci. Numer. Simul. 18, 3530–3557 (2013).
- ²⁹C. Lopesino, F. Balibrea, S. Wiggins, and A. M. Mancho, "Lagrangian descriptors for two dimensional, area preserving, autonomous and nonautonomous maps," Commun. Nonlinear Sci. Numer. Simul. 27, 40–51 (2015).
- 30C. Lopesino, F. Balibrea-Iniesta, V. J. García-Garrido, S. Wiggins, and A. M. Mancho, "A theoretical framework for Lagrangian descriptors," Int. J. Bifurcation Chaos 27, 1730001 (2017).
- ³¹V. J. García-Garrido, "Unveiling the fractal structure of Julia sets with Lagrangian descriptors," Commun. Nonlinear Sci. Numer. Simul. 91, 105417 (2020).
- 32S. C. Shadden, F. Lekien, and J. E. Marsden, "Definition and properties of Lagrangian coherent structures from finite-time Lyapunov exponents in two-dimensional aperiodic flows," Phys. D: Nonlinear Phenom. 212, 271-304 (2005).
- 33S. Norouzi, "Flow characteristics in abdominal aortic aneurysms: An in vitro study," Master's thesis (Concordia University, 2020).
- ³⁴G. D. Labbio and L. Kadem, "Jet collisions and vortex reversal in the human left ventricle." J. Biomech. 78, 155–160 (2018).
- 35G. D. Labbio and L. Kadem, "Reduced-order modeling of left ventricular flow subject to aortic valve regurgitation," Phys. Fluids 31, 031901 (2019).
- 36V. J. García-Garrido, "An extension of discrete Lagrangian descriptors for unbounded maps," Int. J. Bifurcation Chaos 30, 2030012 (2020).
- ⁵⁷See https://github.com/dilabbiog/ROMs-LV_flow_with_AR for "In Vitro Data-Driven Reduced-Order Models of Left Ventricular Flow Subject to Aortic Valve Regurgitation"
- ⁵⁸See https://github.com/AhmedDarwish466/LDCardio for "A MATLAB package for Lagrangian Descriptors evaluation."
- ³⁹See https://github.com/dilabbiog/matfluids for "A MATLAB Package for Processing Fluid Flow Data"